Effective heterogeneous electro-Fenton process for the degradation of a malodorous compound, indole using iron loaded alginate beads as a reusable catalyst

Samia Ben Hammouda, Florence Fourcade, Aymen Assadi, Isabelle Soutrel, Nafâa Adhoum, Abdeltif Amrane, Lotfi Monser

Effective heterogeneous electro-Fenton process for the degradation of a malodorous compound, Indole using iron loaded alginate beads as a reusable catalyst

Samia Ben Hammouda[a,b*], Florence Fourcade[b], Aymen Assadi[b], Isabelle Soutrel[b], Nafaa adhoum[a], Abdeltif Amrane[b], Lotfi Monser[a]

[a]Institut National des Sciences Appliquées et de Technologie, B.P. N°676, 1080 Tunis Cedex, Tunisia
[b]Ecole Nationale Supérieure de Chimie de Rennes, CNRS, UMR 6226, 11 allée de Beaulieu, CS 50837, 35708 Rennes Cedex 7, France
*Corresponding author. Tel.: +21622625196; fax: +21671704329
E-mail address: samiabenhammouda@gmail.com

Highlights

Fe-ABs were fabricated by simple gelation procedure at 25 °C. ► The incorporation of iron on beads was confirmed by EDS results. ► The Fe-ABs catalyst present good stability and can be used for at least four times without obvious decrease in activity. ► Mineralization pathways of indole was proposed.

Graphical abstract

Abstract

In this work the characterization and the performance of iron immobilized in alginate beads (Fe-ABs) as catalyst for heterogeneous electro-Fenton (EF) treatment of a malodorous compound, indole, was investigated. Experimental results demonstrated that indole was effectively removed through the electro-Fenton process; while in the considered experimental conditions, the performances of EF were only slightly improved by the addition of UVA radiation.

The most efficient operating conditions were achieved at pH 3.0 in the presence of 200 mg.L^{-1} Fe-ABs catalyst (corresponding to an average iron concentration of 64 mg L^{-1}) with a current density of 0.53 mA cm^{-2}. Under these conditions, 60 min were sufficient to completely degrade 20 mg L^{-1} of indole, whose removal was found to obey the pseudo-first order model. In terms of organic carbon removal, about 90% mineralization yield was reached in the optimal conditions for 7 h heterogeneous electro-Fenton treatment time.

UPLC–MS/MS analysis was applied to identify and follow the evolution of indole oxidation products. Five stable organics intermediates were observed and four of them were identified as dioxindole, isatin, oxindole and anthranilic acid. A reaction sequence was therefore

proposed for indole degradation according to the detected products. Subsequent attack of these intermediates by •OH radicals led to the formation of short chain acids such as succinic, acetic, oxamic and oxalic identified by ion-exclusion chromatography.

Keywords:

Electro-Fenton; photoelectro-Fenton; iron alginate catalyst; Indole; degradation pathway.

Introduction

Malodorous compounds can be found or can develop in wastewaters, depending on ambient conditions. Most recently, the impact of malodorous on human health has gained further attention and interest of researchers aiming for a better quality of life.

Among various malodorous compounds, indole is ranked as a toxic recalcitrant compound that is considered to be an environmental pollutant. Also, indole is regarded as among the most disgusting and smelly compound usually identified in wastewater [1-8].

Indole can be produced by bacteria as a degradation product of tryptophan in the rumen. It is also produced by industries for different applications, including pharmaceuticals, cosmetics, pesticides, agrochemicals, and dyestuffs [9].

Biodegradation have been widely used for remedying indole from aqueous solutions with pure strains bacteria (Alcaligenes, Pseudomonas genus) or fungi (Sporotrichum, Phomopsis genus) [10-12]. However, biodegradation takes several days or weeks [13, 14] and therefore cannot be used in sites where immediate action is required. Thus, rapid and efficient treatment processes must be developed for indole removal.

Electrochemical advanced oxidation processes (EAOPs) such as anodic oxidation (AO) [15-18], electro-Fenton (EF) and photoelectro-Fenton (PEF) [19-26] have proven to be efficient for removing organic matter. These processes are considered environmentally friendly and they are based on the in situ electrochemical generation of hydroxyl radicals (•OH), which is

the second strongest oxidant known after fluorine, with $E°$ (•OH / H_2O) = 2.8 V vs.SHE (Standard Hydrogen Electrode) [27].

The electro-Fenton process is based on the continuous supply of H_2O_2 to the contaminated solution from the two-electron reduction of dissolved O_2 gas at the cathode (Eq1). A catalytic amount of Fe^{2+} is added to the solution to react with H_2O_2 to yield the strong homogeneous oxidant •OH and Fe^{3+} from the well-known Fenton's reaction (Eq2). Compared to the conventional Fenton method, the electro-Fenton method offers the advantages of avoiding the storage and the transportation of hydrogen peroxide. Ferrous ions are added in catalytic amount thanks to their recycling by electrochemical reduction of produced ferric ions (Eq3); the production of iron hydroxide sludge is then lower compared to the classical Fenton's reaction.

$$O_2\,(gas) + 2H^+ + 2e^- \rightarrow H_2O_2 \qquad \textit{(Eq 1)}$$

$$Fe^{2+} + H_2O_2 \rightarrow Fe^{3+} + \bullet OH + OH^- \qquad \textit{(Eq 2)}$$

$$Fe^{3+} + e^- \rightarrow Fe^{2+} \qquad \textit{(Eq 3)}$$

The efficiency of the electro-Fenton process can be improved if the solution is simultaneously irradiated with UVA light illumination, giving rise to the photoelectro-Fenton process. Compared to the electro-Fenton process, its degradation performances are higher and a total mineralization can be reached [28-33].

In the presence of UV radiations, additional sources of •OH radicals should be considered through UV radiations interaction with the iron species in aqueous solutions, mainly the photoreduction of $Fe(OH)^{2+}$, which allows the generation of Fe^{2+} and •OH as shown in reaction 4 (eq 4) [34-37].

$$Fe\,(OH)^{2+} + h\,\nu \rightarrow Fe^{2+} + \bullet OH \qquad \textit{(Eq 4)}$$

The catalytic action of UV irradiation can be also explained by the quick photolysis of the recalcitrant Fe (III)–carboxylate complexes according to the general reaction (Eq 5) [36]. The rapid photolysis of these persistent intermediates by UVA light improves their mineralization rate.

$$Fe\,(OOCR)^{2+} + h\,\nu \rightarrow Fe^{2+} + CO_2 + R^{\bullet} \qquad (Eq\ 5)$$

In recent years, great effort have been undertaken to develop active heterogeneous catalysts in order to promote Fenton chemistry. The heterogeneous system offers several advantages over its homogeneous counterpart, such as the prevention of sludge formation, the possibility of recycling the iron promoter and its easy separation [38, 39].

Among various heterogeneous Fenton catalysts, iron embedded in alginate gel beads have shown high catalytic activities for the oxidation of organic compounds. The use of alginate as biopolymer matrix for iron immobilization can be advantageous due to its well known biocompatibility, biodegradability, abundance, lower price and ease of processing [40-44].

In the present study, the degradation of indole was investigated with heterogeneous electro-Fenton process using iron supported alginate beads (Fe-ABs). Initially the characterization of Fe-ABs was performed. The influence of current intensity, catalyst dosage on indole and mineralization yields was examined. The integration of UVA irradiation simultaneously to the electrochemical process in the same reactor was also tested.

The degradation of indole by heterogeneous electro-Fenton and its degradation intermediates were followed by chromatographic techniques (HPLC, UPLC–MS/MS and ion-exclusion chromatography). A general reaction sequence for indole mineralization involving all detected products was proposed. Finally, a special attention was devoted to the reusability of the Fe-ABs catalysts.

2. Experimental set up

2.1. Chemicals products

All chemicals and solvents were of analytical grade and used without further purification. Indole was obtained from ACROS Organics (Geel, BE), sodium alginate and Iron (II) sulfate were purchased from PROLABO (Paris, Fr). Calcium chloride and acetonitrile (HPLC-grade) were purchased from Fisher Scientific (Loughborough, UK). Sodium sulfate was obtained from Merck (Paris, Fr).Ultra-pure water obtained from ELGA Purelab Option-Q DV 25system was utilized for the preparation of all working solutions, as well as HPLC and LC–MS/MS mobile phases. The initial pH of solutions was adjusted using analytical grade sulfuric acid supplied by Merck (Paris, Fr).

2. 2. Electrochemical cell

Heterogeneous electro-Fenton and photoelectro-Fenton experiments were performed at room temperature (25 ± 1 °C) in an undivided closed glass cell at current controlled conditions. The electrochemical cell was monitored by a power supply MICROLAB Micronic System (Villetted'anthon, Fr).

The dimensions of the carbon felt piece (Mersen, Paris, Fr), which was used as the working electrode (cathode), were (5 x 5 cm). Its specific area, measured by the BET method was 0.7 $m^2\ g^{-1}$, its thickness was 1.2 cm, its density was 0.088 g cm^{-3} and its carbon yield was 99.9 %. The counter electrode (anode) was a cylindrical platinum grid of about 5 cm^2 (5 cm x 1 cm), which was centered in the cell and surrounded by cathode covering the inner wall of the cell.

In all experiments, the pH of the solutions was adjusted to 3.0 by sulfuric acid. The ionic strength was maintained constant by the addition of an inert supporting electrolyte (Na_2SO_4).

All electrolysis experiments were conducted under continuous compressed air bubbling in order to ensure continuous production of hydrogen peroxide via oxygen reduction at the

cathode surface. Prior to electrolysis, compressed air was bubbled for 15 min through the solution to saturate the aqueous solutions, which were agitated continuously by a magnetic stirrer. Subsequently, the treatment was initiated by applying a constant current density under continuous compressed air bubbling at about 0.25 L min^{-1}.

The photoelectro-Fenton experiments were carried out using an UV-A lamp 24 W (Philips PL-L) placed between the two electrodes in the center of the glass cell emitting in a wavelength region 320 - 400 nm with emission peak centered at λ_{max} = 360 nm, yielding a photoionization energy of 60 W m^{-2} as detected with a UV Radiometer (VLX- 3W equipped with a sensor CX 365, ALYS Technologies, Switzerland). The location of the two electrodes was therefore modified in comparison to the heterogeneous electro-Fenton process.

The heterogeneous electro-Fenton and photelectro-Fenton were performed with iron immobilized on alginate beads (Fe-ABs), which played the role of catalyst. A catalytic quantity of Fe-ABs was introduced to the cell just before beginning of the electrolysis.

2. 3. Preparation of Fe alginate beads

Iron was loaded on alginate by a wet impregnation technique. Sodium alginate solution (3.0 % w/w) was prepared by dissolving an appropriate amount of alginic acid sodium salt in distilled water, which was then added drop wise into a hardening solution composed of 0.5 mol L^{-1} Ca^{2+} ($CaCl_2$.$2H_2O$) and 0.1 mol L^{-1} Fe^{2+} ($FeSO_4$.$6H_2O$). A syringe needle was used to produce the spherical Fe-ABs (Fig.1a) at a dropping rate of approximately 1.0 mL min^{-1}.

2.4. Analysis procedures

2.4.1. HPLC analysis

The concentration of indole was quantified using a Waters High Performance Liquid Chromatography (HPLC) equipped with a C18 reverse-phase Column (4.6 mm x 250 mm, 5 µm) and an AutoSampler Injector (Waters 717). Prior to injection, the samples were filtered

through a 0.45 μm filter. The injection volume was set at 50 μL and an isocratic eluent water/Acetonetrile (40/60, v/v) was pumped at a flow rate of 1.0 mL min^{-1}. Indole had a retention time of 5.7 min under these conditions.

Detection was performed with a photodiode array detector (Waters 996) at 270 nm and the column temperature was maintained at 25 °C with a column thermostat.

Generated carboxylic acids, nitrate and nitrite ions were identified and quantitatively followed by ion exclusion chromatography using a DIONEX DX120 ion chromatography system equipped with a conductivity detector. An IonPac (4mm × 250 mm) was used as anion exchange column. The eluent was a Na_2CO_3 (9 mM) solution at a flow rate of 1.0 mL min^{-1}. The determination of NH_4^+ ions was carried out by ion chromatography using a Metrohm 761 Compact IC system fitted with a conductimetric detector and a Shodex cationic column IC YK-421 under isocratic elution of 18 mM methanesulfonic acid (MSA) as mobile phase at flow rate 1.0 mL min^{-1}.

2.4.2. UPLC–MS/MS analysis

To identify the by-products obtained during the indole degradation, several samples were analyzed by ultra-high pressure liquid chromatography (Acquity UPLC – Waters) coupled to mass spectrometry Tandem (Triple Quad Quattro Premier Waters).

The analytes were separated by the Waters Acquity UPLC system consisting of an Acquity UPLC binary solvent manager, an Acquity UPLC sample manager and an Acquity UPLC column heater equipped with a Waters Acquity UPLC BEH C18 column (2.1 × 100 mm, 1.7 μm particle size) (Milford, MA, USA). Isocratic LC elution was performed with acetonitrile quality LC-MS as mobile phase A and an ultrapure water 9:1 acetonitrile (v/v) mixture as mobile phase B. Separation of the analytes on the column was performed at 0.4 mL min^{-1} flow rate.

A mass spectrometer (Micromass, Manchester, UK) equipped with an electrospray ionization source was used for degradation products detection. MS/MS detection was performed in negative and positive mode. The tension of the capillary was set to 3000V. The temperatures of the source and the desolvation gas were set at 120 and 350°C, respectively. The cone and desolvation gas flows (N_2) were 50 and 750 L h^{-1}, respectively. High-purity argon (99.99%, Air Liquid, Paris, France) was used as collision gas. The analytical device was controlled by MicromassMassLynx 4.1 software.

2.4.3. Non-Purgeable Organic Carbon (NPOC) measurements

The progress of the mineralization of indole aqueous solutions during the treatment was monitored by measuring their non-purgeable organic carbon (NPOC) abatement. Samples were periodically withdrawn at different time intervals and were filtered onto hydrophilic membranes (Sartorius Stedim Minisart, pore size 0.40 μm).

The NPOC in samples was measured by means of a TOC-VCPH/CPN Total Organic Analyzer Schimadzu. Organic carbon compounds were combusted and converted to CO_2, which was detected and measured by a non-dispersive infrared detector (NDIR). Standard potassium hydrogen phthalate solutions were used as standards for the NPOC analysis. For each sample, each measurement was duplicated.

2. 4. 4. Iron content and morphology of beads

The morphology of the synthesized catalyst (Fe-ABs) was evaluated by scanning electron microscopy (SEM). SEM was performed on a field effect JEOL JSM-6301F equipped with an EDS Oxford Inca Energy 300 SEM at an accelerating voltage of 15 kV. Microanalysis by energy-dispersive spectroscopy (EDS) was performed with a JEOL model JSM 6400 (Oxford INCA).

The specific surface area (SSA) was carried out by nitrogen gas adsorption at 77 K after out gassing at 120 °C under helium gas, using a Quantachrome-Autosorb-1 sorptiometer. The specific area was calculated by the BET method.

In order to determine the Fe content immobilized on the Fe alginate gel beads, 100 beads were selected randomly and treated with 6.0 mol L^{-1} H_2SO_4 aqueous solution at room temperature for 24 h. Iron ions were released from Fe alginate gel beads and their concentration in the solution was determined by using an atomic absorption spectrometer (AA140, VARIAN), for calculating the total Fe content of the beads.

Total dissolved iron (Fe (II) + Fe (III)) can also be determined by the orthophenonthroline complexometric method [45], which based on the reduction of Fe (III) to Fe (II) using the reducing agent hydroxylamine hydrochloride ($NH_2OH.HCl$). To determine the amount of dissolved ferrous iron in solution, this reducing agent was omitted. The concentration of dissolved Fe (III) was then calculated as the difference between total iron and ferrous iron.

3. Results and discussion

3.1. Catalyst characterization

The specific surface area of the alginate beads was determined by the BET method and was found to be 9.32 m^2 /g.

Using an acid digestion it was determined that the used Fe alginate beads have a Fe concentration of 320 mg g^{-1}. The average content of iron for a single bead is estimated to be 0.40±0.03 mg (Table1). Moreover, it was found that the supported catalyst (Fe-ABs) contains both ferrous and ferric ions with a percentage of 69.17 and 30.83 %, which corresponding to 221.34 and 98.68 mg g^{-1}, respectively.

Morphological examination of the surface and internal structure of the dried beads was also carried out. A scanning electron micrograph (SEM) and the energy-dispersive X-ray

spectroscopy (EDS) analysis of the synthesized Fe-alginate beads are shown in Fig.1.Scanning electron microscopy revealed that the beads were spherical in shape with rough surface. SEM micrograph showed the egg-box structure resulting of the ionic cross-linking between alginate and calcium ions during the gelation process.

X-ray emission peaks are labeled (Fig.2). A strong signal corresponding to Fe was observed in the spectrum confirming the presence of iron in the biopolymer matrix with a weight percentage of 42 %.

Figure 1

Figure 2

Table 1

3.2. Oxidation of indole in aqueous solutions

3. 2. 1. Study of indole degradation by heterogeneous electro-Fenton

Taking into account the possible adsorption of indole on alginate beads, adsorption studies were initially carried out. The adsorption of indole onto alginate beads was investigated in the absence of an electrical field. Fig.3a showed that after 1 h contact time with the beads, the amount of indole adsorbed was lower than 5 %. Subsequently, the degradation of indole by heterogeneous electro-Fenton process (EF-Fe-ABs) was carried out by electrolyzing 20 mg L^{-1} indole solutions at 0.53 mA cm^{-2} with 200 mg L^{-1} of Fe-ABs catalyst (Fig. 3a). Under these conditions, complete disappearance of indole was occurred after 60 min of electrolysis. Results revealed that the degradation of indole was well-fitted to a pseudo-first-order reaction with the apparent kinetic coefficient k_{app} = 1.13 x 10^{-3} s^{-1} and a regression coefficient higher than 99% (Fig. 3b).

Possible catalytic oxidation mechanism of the heterogeneous electro-Fenton process

The heterogeneous electro-Fenton reaction is a surface-controlled process which depends mainly on hydrogen peroxide concentration and the supported catalyst properties. Until now, its reaction mechanism was not agreed upon. However, it is commonly recognized that the production of hydroxyl radical from the decomposition of hydrogen peroxide catalyzed by the supported iron entities is the critical step in the entire oxidation process, which fits the Harber-Weiss circle mechanism similarly to the mechanism of the classic homogeneous electro-Fenton reaction [47-49].

According to the work of Rosales et al [41], the distribution of iron on the alginate beads surface was homogeneous. Hydrogen peroxide produced at the cathode came into contact of Fe (II) on the beads surface to produce Fe (III) and hydroxyl radicals. It should be pointed out that, throughout experiments, compressed air sparging into the solution in addition to a mechanical agitation of the solution allowed the contact of the Fe-alginate beads on the cathode surface. During this contact, Fe (III) present on the beads surface can be reduced [46]. Moreover according to the mechanism of heterogeneous electroFenton, Fe (III) can react with hydrogen peroxide to regenerate Fe (II) [50] following the reaction 6 (Eq 6):

$$Fe^{3+} + H_2O_2 \rightarrow Fe^{2+} + HO_2\bullet + H^+ \qquad \textit{(Eq 6)}$$

Effect of UV irradiation

For comparative purpose and in an attempt to further improve the heterogeneous electro-Fenton reaction kinetic, the effect of UV-illumination on the EF degradation of indole was investigated (Fig. 3a) with 200 mg L^{-1} of Fe-Abs at 0.53 mA cm^{-2}. Results revealed that the degradation of indole was also well-fitted to a pseudo-first-order reaction with a regression coefficient higher than 99% but in the study operating conditions, photoelectron-Fenton did not improve significantly the indole oxidation in contrast with results from the literature.

As shown in Fig 3a, one can infer a slight synergistic effect for the combination between electro-Fenton and UV radiation. The kinetic apparent rate constant was increased from 1.13 x 10^{-3} to 1.19 x 10^{-3} s^{-1}. This evidences a high photostability of indole under UVA illumination, which is in accordance with the result of Samah et al. [51]. We can conclude that indole was degraded by the action of hydroxyl radicals which are produced mainly by the electrochemical process. This result is in accordance with some other studies which have also reported a slightly improvement in the performance of electro-Fenton process when combined with UV irradiation [37] [52-59]

Taking into account the limited improvement of the performances obtained with PEF compared to EF system and the high energy requirements of PEF related to both the electrochemical cell and the UVA lamp, we thought that for water treatment contaminated with indole in a large-scale system, the heterogeneous electro-Fenton treatment would be most favored.

Figure 3

3.2.2. Effect of the Fe-ABs dosage

The catalyst dosage plays an important role in the heterogeneous electro-Fenton process since it controls the •OH production from the Fenton's reaction (Eq.2).

Thus, in an attempt to optimize the concentration of the heterogeneous catalyst (Fe-ABs), indole removal was investigated at 0.53 mA cm^{-2} and various catalyst concentrations ranging from 50 mg L^{-1} to 250 mg L^{-1} (corresponding to apparent Fe concentrations from 16 to 79 mg L^{-1}). The results are shown in Fig.4.

Notably, the rise in the catalyst content had a positive effect on the degradation profile, since indole removal yields were in the range 66.8 to 100% after 60 min reaction for Fe-ABs

amounts in the range 50 mg L^{-1} to 250 mg L^{-1}. It should be observed that above 150 mg L^{-1} Fe-ABs, there was no significant improvement of the removal yield.

Figure 4

As seen in Fig.4, the apparent kinetic coefficient increased with increasing Fe-ABs dosage up to 200 mg L^{-1}; while the apparent kinetic coefficient decreased above this value. The increasing values of apparent kinetic coefficients with the addition of iron were attributed to the increase in consumption of H_2O_2 leading a higher concentration of hydroxyl radical; while the decrease of the apparent kinetic coefficient can be explained by the fact that radical hydroxyl can be recombined with ferrous ions following the reaction (Eq 7):

$$Fe^{2+} + \bullet OH \rightarrow Fe^{3+} + OH^- \qquad (Eq\ 7)$$

3.2.3. Effect of the applied current density

The current density is a key factor that had notable influence on the reaction rate of electrochemical processes, since it affect both the generation of H_2O_2 and the regeneration of Fe^{2+}. This, in turn, affect the generation of •OH via the Fenton reaction which is proportional to both iron and H_2O_2 concentration, as shown in the following Eq. (8) [60, 61].

$$[\bullet OH] = \lambda\,(d[\bullet OH]/dt) = \lambda\, k_2 [Fe^{2+}][H_2O_2] \qquad (Eq\ 8)$$

Where k_2 is the second-order rate constant of reaction (2); λ is the average life of the •OH; and $[Fe^{2+}]$ and $[H_2O_2]$ are the concentrations of ferrous ion and hydrogen peroxide, respectively.

Following the study of Fontmorin et al. [62], from BET analysis and the felt density (given by the manufacturer), 0.7 $m^2\ g^{-1}$ and 0.088 g cm^{-3}, respectively, the BET surface was 109 times high than the geometrical surface. However, it can be observed that the surface given by the

BET is most likely overestimated, since deduced from the adsorbed nitrogen amount; while and owing to its low size, nitrogen can penetrate pores which are not accessible to water. So the electrochemical electrode surface was determined. From this study, the electrochemical surface of the carbon felt surface is 376 cm^2. The densities current in the text were then deduced from this electrochemical surface.

Fig. 5 shows the effect of applied current density, from 0.13 to 0.80 mA cm^{-2}, on the indole removal. The treatments were performed with 20 mg L^{-1} indole solutions at pH 3.0, in the presence of 200 mg L^{-1} Fe-ABs. The obtained results indicate clearly, as expected, that a more rapid decay of indole can be achieved upon increasing the applied current density.

This behavior can be mainly attributed to a faster production of H_2O_2 and a faster regeneration of ferrous ions, at higher current, leading to a higher generation of hydroxyl radicals.

About 65%, 85%, 96% and 100 % abatement of indole were achieved, after 1 h electrolysis, with current densities of 0.13, 0.26, 0.40 and 0.53 mA cm^{-2}, respectively (Fig.5a). The corresponding rate constants (k_{app}) were 0.34 x 10^{-3}, 0.55 x 10^{-3}, 0.85 x 10^{-3} and 1.13 x 10^{-3} s^{-1}, respectively (Fig.6b).

No further increase of the percentage of indole removal was observed for applied current density beyond 0.53 mA cm^{-2}. It could be explained by some parasitic reactions. When the current intensity increase, the 4 electrons reduction of oxygen (Eq 9) can become predominant compared to the formation of hydrogen peroxide. The high current intensities favor also the production of hydrogen (Eq 10). Moreover parasitic reactions also involve hydrogen peroxide and hydroxyl radicals (Eq 11 to 13) [63- 66]:

$$O_2 + 4\,H^+ + 4\,e^- \rightarrow 2\,H_2O \qquad \textit{(Eq 9)}$$

$$2\,H^+ + 2\,e^- \rightarrow H_2 \qquad \textit{(Eq 10)}$$

$$Fe^{2+} + {\bullet}OH \rightarrow Fe^{3+} + OH^- \qquad \textit{(Eq 11)}$$

$$2\ {\bullet}OH \rightarrow H_2O_2 \qquad \textit{(Eq 12)}$$

$${\bullet}OH + H_2O_2 \rightarrow {\bullet}O_2H + H_2O \qquad \textit{(Eq 13)}$$

Figure 5

3.2.4. Indole mineralization by heterogeneous electro-Fenton

Since some intermediates by products were formed and accumulated during each treatment, the monitoring of the target compound degradation has to be completed by the examination of mineralization time-course, which is displayed in Fig.6.

Figure 6

Fig.6 highlights that 88% NPOC removal was achieved after 6 h of electrolysis at 0.53 mA cm^{-2} with EF-Fe-ABs (Fig.6a). At the time of the complete removal of indole, namely after 60 min of treatment, about 38% of mineralization was achieved. Moreover, it is interesting to note that the decay rate was faster up to 180 min of electrolysis and tended to decrease during the course of electrolysis. At the beginning of the oxidation, only the target compound and a few amounts of by products were attacked by hydroxyl radicals. The attack by hydroxyl radicals was not selective and several byproducts were generated all along the oxidation process and a competition between the oxidation of these compounds took place, inducing a decrease of the mineralization rate.

When the heterogeneous Electro-Fenton treatment has been combined with UV irradiation, the mineralization efficacy has slightly improved, reaching 93% after 6h of PEF treatment. One should note that this improvement was more pronounced at the beginning of the treatment.

This result leads us to conclude that indole intermediates are probably recalcitrant to the UV photolysis. Also, the observed lack of significant influence of UV irradiation points out its negligible effect on ferrous ions regeneration and hydroxyl radical production through Eq (5). Besides purely chemical reasons, the slight synergistic effect observed could be also ascribed to the fact that the configuration of the integrated process may not provide a good irradiation of the medium due principally to the wrong position of the lamp between the two electrodes which leads to the loss of a major part of the irradiation. Moreover, the lamp position could also affect the mass transfer of alginate beads to the electrode surface which in turn negatively affects the efficacy of the electro-Fenton treatment.

According to NPOC data, the mineralization current efficiency (MCE) at a current I (A) and a given electrolysis time t (h) can be estimated as follows [67-69]:

$$MCE, \% = 100\frac{nFV\Delta(NPOC)exp}{4.3210^7 mIt} \qquad (Eq\ 14)$$

Where n is the number of electrons consumed in the mineralization process, F is the Faraday constant (96487 C mol^{-1}), v is the solution volume (L), $\Delta(NPOC)_{exp}$ is the experimental NPOC decay (mg L^{-1}), 4.32 x 10^7 is a conversion factor, m is the number of carbon atoms of indole (8), I is the applied total current (A) and t the electrolysis duration (h).

The number of electrons (n) consumed per each indole molecule was considered to be 44, assuming that its overall mineralization leads to carbon dioxide and nitrate ions as follows:

$$C_8H_7N + 19\ H_2O \rightarrow 8\ CO_2 + NO_3^- + 45\ H^+ + 44\ e^- \qquad (Eq\ 15)$$

In a previous study, González-Vergas et al [65] obtained a maximum value of 25% during the electro-Fenton mineralization of 100 mg L^{-1} of Acid red. In this study, at 80 mA cm^{-2}, low values of MCE were obtained with maximum values of 6.6 % and 8.4% (fig.6) for heterogeneous electro-Fenton and photoelectron-Fenton respectively. Indeed, the total amount of catalyst was not necessary available and compared to free ferrous ions in solution, mass

transfer can be also limited by the reaction of hydrogen peroxide at the surface of Fe-ABs and a probably lower regeneration of ferrous ions.

Moreover, it is interesting to note that the MCE values underwent a dramatic decay at long electrolysis time of EF and PEF, which can be explained mainly by the formation of resistant intermediates and the limitations related to low organic loads [29].

The effect of the applied current density on the mineralization during EF experiments was also studied and the results are depicted in Fig.7a. A gradual increase in NPOC abatement was observed for increasing applied currents, due to the larger amount of hydroxyl radicals produced via Eq.1, as also observed for the target compound degradation (Fig.5). NPOC removal achieved nearly 90% yield after 6 h of treatment at 80 mA cm^{-2}, showing that indole and almost all its organic intermediates were completely mineralized to CO_2, water and inorganic ions.

In addition, Fig 7c highlighted a decrease of MCE with the current density, from 16% at 0.27 mA cm^{-2} to 6.6% at 0.80 mA cm^{-2}, thus confirming the waste of radicals in self-destruction and other side reactions at high current density [69].

For all applied current densities, we note that MCE tends to decrease at long electrolyses time, which can be ascribed to the production of more resistant intermediates and to the mass transport limitations related to low organic loads [69].

Figure 7

In order to determine whether the process is likely to be efficient and powerful, the electrical consumption of energy during the removal of indole was also studied. Energy consumption (kWh g^{-1}), defined as the electrical energy required to remove 1 g of NPOC, was calculated from the following equation [33] [70, 71]:

$$EC_{NPOC}\ (kWh.g^{-1}\ NPOC) = \int_0^t \frac{E_{cell}\, I}{V_s\, d(NPOC)_{exp}}\, dt \qquad (Eq\ 16)$$

Where E_{cell} is the average potential difference of the cell (V), I the applied current (A), t the duration of electrolysis (h), Vs the solution volume (L) and $(NPOC)_{exp}$ the experimental NPOC decay (mgL^{-1}).

As shown in Fig.7b, more energy consumption (EC, in $kWhg^{-1}$ NPOC indole) was required when the applied current intensity increased. Indeed, to obtain about 60 % NPOC removal, the EC value increased only from 0.75 $kWhg^{-1}$ NPOC indole at 0.27 mA cm^{-2} to 0.87 $kWhg^{-1}$ NPOC indole at 0.53 mA cm^{-2}. It is noteworthy that increasing the current density above 0.53 mA cm^{-2} led to a drastic increase of the energy consumption, 1.92 kWh/g NPOC for 60% NPOC removal at 0.80 mA cm^{-2} (Fig 7a and b) , while no significant increase regarding NPOC removal can be observed compared to 0.53 mA cm^{-2} Fig.7a). From this, 0.53 mA cm^{-2} appeared viable for industrial application, leading to 2.06 kWh g^{-1} NPOC to achieve 90.03 % mineralization yield for 7h electro-Fenton treatment time (Fig.7). On the contrary, a current density of 0.80 mA cm^{-2} was not appropriate in these operating conditions since not only the mineralization yield was similar to that obtained at 0.53 mA cm^{-2} but also both MCE and EC values reached the worst process performances.

3. 3. Identification and evolution of indole by-products during EF-Fe-ABs process

HPLC analysis indicated that the indole oxidation by hydroxyl radicals led to the gradual disappearance of the parent molecule (indole) and the formation of different intermediate compounds. These by-products were identified by LC–MS/MS analysis in order to elucidate a plausible reaction pathway of the heterogeneous electro Fenton oxidation. Taking into account that the removal of indole under higher current values was much faster, trial was carried out at 0.27 mA cm^{-2} in order to avoid the fast degradation of the indole intermediates. Furthermore, the corresponding experiment was conducted at high concentration (200 mg L^{-1}) in order to ensure their detection. The initial solution and samples from different treatment times at pH 3.0 were analyzed. The identification was based on mass fragmentation values

and by comparing the mass spectra to a database. The main compounds generated during the electro-Fenton treatment were described in Table 2.

Table 2.

Fig. 8 shows the LC–MS/MS profiles of indole and its derivatives at different treatment times. As observed, the decrease of the concentration of indole is accompanied by an increase of its derivatives with treatment time. The final analysis of samples after 5 h of electro-Fenton treatment indicated the complete removal of all these compounds. Further oxidation of these derivatives under electro-Fenton process led to the formation of short chain carboxylic acids which are the last by-products before mineralization, Oxalic acid (tr = 19.9 min), acetic acid (tr = 7.62 min), oxamic acid (20.16 min) and succinic acid (tr = 19.63 min) were the main acids identified by ion chromatography in the final stage of indole degradation; their retention times were compared with standard compounds. Even after 480 minutes, the total mineralization of oxalic acid did not occur (data not shown).

In addition, the initial nitrogen present in the target compound can be converted into nitrate (NO_3^-) and hence identified by its retention time (tr = 13.7 min) using ion exchange chromatography. In contrast, the nitrite ion (NO_2^-) was not detected.

Furthermore, cationic analysis showed that a negligible amount of NH_4^+ was detected in the samples. Nevertheless, this result does not prove that a greater amount of ammonium ions were not formed during the E-F treatment. Indeed, ammonium ions could have been quickly adsorbed at the surface of alginate beads. This assumption could be supported because alginate beads have high affinity for adsorption of cations (mainly metal cations). Also, Bashana et al. have reported a significant increase in the removal of ammonium by the co-immobilization of alga onto alginate beads [72]. A good NH_3 adsorption capacity by pure calcium alginate beads has been also reported by Chung et al. [73].

A plausible mineralization sequence was proposed for indole removal during the electro-Fenton process on the basis of the above intermediates. The main initial reaction was the electrophilic addition of a hydroxyl radical on the aromatic ring. As shown in Fig.9 the first step of indole degradation was a hydroxylation in position 2, leading to the formation of 2-oxindole. The second hydroxylation was in position 3, which led to the production of Isatin (indole-2,3-dione). The reduction of dioxindole to anthranilic acid was the final step prior to the ring-opening and the formation of short chain carboxylic acids. This pathway was in accordance with studies reported by Johansen et al. [74] for an anaerobic degradation by Desulfobacterium indolicum. Many of these compounds are also found in other microbial degradation processes [75].

Figure 8

Figure 9

3.5. Fe-ABs Recyclability

The reusability of the used catalyst is an important factor in the development of heterogeneous electro-Fenton treatment. To analyze the applicability of the developed catalyst to operate in successive cycles, several electro-Fenton treatments were successively carried out under the same conditions considered in the first cycle. As can be seen in Fig.10, the catalyst can be reused at least four times without loss of activity. Similar results were obtained by Rosales et al. [41] during the electro-Fenton oxidation of azo-dyes. Their results showed that the time for a total decolorization increased after three cycles. On the other hand, Iron leaching was evaluated during the assays and it was not detected in the liquid supernatant. These results confirmed the good stability of the Fe-ABs.

Figure 10

Conclusion

In view of the results obtained, it can be concluded that the studied indole can be effectively treated by the heterogeneous electro-Fenton process using Fe alginate beads as catalyst.

The optimum amount of iron alginate beads (Fe-ABs) was found to be 200 mg L^{-1}, complete indole removal was observed within 60 min at an initial pH of 3.0 and a current intensity of 0.53 mA cm^{-2}.

In terms of organic carbon removal, about 90% mineralization yield was reached in the optimal conditions after 7 h of heterogeneous electro-Fenton treatment time.

A kinetic analysis showed that the removal of indole by EF-Fe-ABs followed a first-order kinetics model (k_{app} = 1.13 x 10^{-3} s^{-1}).

Five intermediates by-products were identified and their evolution during the electro-Fenton treatment was followed. The identification and the follow-up of the oxidation products and short-chain carboxylic acids led to the proposal of a degradation pathway for indole via hydroxyl radicals. Beads recyclability was shown since they can be reused at least four times without iron leaching.

Acknowledgements

This work was supported by the Tunisian Ministry of Higher Education and Scientific Research and the authors wish to thank it.

REFERENCES**s**

[1] M. Ochiai, K. Wakabayashi, T. Sugimura, M. Nagao, Mutat. Res. 172 (1986) 189 –197.

[2] N. Doukyu, R. Aono, Extremophiles. 1 (1997) 100 –105.

[3] S. Fetzner, Appl. Microbial. Biotechnol. 49 (1998) 237–250.

[4] A. V. Kamath, C. S. Vaidvanathan, Appl. Environ. Microbiol. 56 (1990) 275 –280.

[5] L. J. Yuan, J. B. Liu, X. G. Xiao, Afr. J. Biotechnol. 10 (2011) 19855 –19863.

[6] D. F. Berry, E. L. Madsen, J. M. Bollag, Appl. Environ. Microbiol. 53 (1987) 180 –182.

[7] Y. T. Wang, M. T. Suidan, J. T. Pfeffer, Appl. Environ. Microbiol. 48 (1984) 1058 –1060.

[8] V. N. Burd, R. Bantleon, K. H. Van Pee, Appl. Biochem. Micro. 37 (2001) 248 –250.

[9] F. Bak, F. Widdel, Arch. Microbiol. 146 (1986) 170 –176.

[10] M. Fujioka, H. Wada, Biochim. Biophys. Acta. 158 (1968) 70 –78.

[11] G. Claus, H. J. Kutzner, Syst. Appl. Microbiol. 4 (1983) 169 –180.

[12] B. Yin, J. D. Gu, N. Wan, Int. Biodeter. Biodegr. 56 (2005) 243 –248.

[13] P. Katapodis, M. Moukouli, P. Christakopoulos, Int. Biodeter. Biodegr. 60 (2007) 267 –272.

[14] Y. Chen, X. G. Xie, C. G. Ren, C. C. Dai, Bioresour. Technol. 129 (2013) 568 –574.

[15] N. B. Tahar, A. Savall, J. Electrochem. Soc. 145 (1998) 3427 –3434.

[16] X. Chen, G. Chen, Sep. Purif. Technol. 48 (2006) 45 – 49.

[17] E. Brillas, I. Sirés, C. Arias, P. L. Cabot, F. Centellas, R. M. Rodríguez, J. A. Garrido, Chemosphere. 58 (2005) 399 – 406.

[18] J.M. Aquino, R.C. Rocha-Filho, N. Bocchi, S.R. Biaggio, J. Appl. Electrochem. 40 (2010) 1751–1757.

[19] M. Pimentel, N. Oturan, M. Dezotti, M. A. Oturan, Appl. Catal. B: Environ. 83 (2008) 140 –149.

[20] B. Balci, N. Oturan, R. Cherrier, M. A. Oturan, Water Res. 43 (2009) 1924 –1934.

[21] M. Panizza, G. Cerisola, Water Res. 43 (2009) 339 – 344.

[22] A. El-Ghenymy, J. A. Garrido, F. Centellas, C. Arias, P. L. Cabot, R. M. Rodríguez, Brillas, J. Phys. Chem. A. 116 (2012) 3404 – 3412.

[23] S. Garcia-Segura, J. A. Garrido, R. M. Rodríguez RM, P. L. Cabot, F. Centellas, C. Arias, E. Brillas, Water Res 46 (2012) 2067–2076.

[24] I. Sirés, C. Arias, P. L. Cabot, F. Centellas, J. A. Garrido, R. M. Rodríguez, E. Brillas, Chemosphere. 66 (2007) 1660 –1669.

[25] N. Oturan, H. Khalaf, M. A. Oturan, Procedia. Eng. 33 (2012) 181–187.

[26] G. Kaichouh, N. Oturan, M. A. Oturan, A. El Hourch, K. El Kacemi, Environ. Technol. 29 (2008) 489 – 496.

[27] N. Borràs, C. Arias, R. Oliver, E. Brillas, J. Electroanal. Chem. 689 (2013) 158 –167.

[28] J. Anotai, S. Singhadech, C.C. Suc, M. C. Luc, J. Hazard. Mater. 196 (2011) 395– 401.

[29] H. Olvera-Vargas, N. Oturan, M. A. Oturan, E. Brillas, Sep. Purif. Technol. 146 (2015) 127–135.

[30] W. P. Ting, M. C. Lu b, Y.H. Huang, J. Hazard. Mater. 156 (2008) 421–427.

[31] J. J. Pignatello, E. Oliveros, A. MacKay, Crit. Rev. Environ. Sci. Tech. 36 (2006) 1–84.

[32] I. T. Peternel, N. Koprivanac, A. M. L. Boˇzi´c, H. M. Kuˇsi´c, J. Hazard. Mater. 148 (2007) 477– 484.

[33] E. Brillas, J. Mex. Chem. Soc. 58 (2014) 239– 255.

[34] F.C. Moreira, S. Garcia-Segura, R. A. R. Boaventura, E. Brillas, V. J. P. Vilar, Appl. Catal. B: Environ. 160-161 (2014) 492–505.

[35] S. Garcia-Segura, A. El-Ghenymy, F. Centellas, R.M. Rodriguez, C. Arias, J. A. Garrido, P. L. Cabot, E. Brillas, J. Electroanal. Chem. 681 (2012) 36 – 43.

[36] F. C. Moreira, S. Garcia-Segura, V. J. P. Vilar, R.A.R. Boaventura, E. Brillas, Appl. Catal. B: Environ. 142-143 (2013) 877– 890.

[37] X. Florenza, A. M. S. Solano, F. Centellas, C.A. Martínez-Huitle, E. Brillas, S. Garcia-Segura, Electrochim. Acta. 142 (2014) 276 – 288.

[38] R. C. C. Costa, F. C. C. Moura, P. E. F. Oliveira, F. Magalhães, J. D. Ardisson, R. M. Lago, Chemosphere. 78 (2010) 1116 – 1120.

[39] O. Iglesias, M.A.F. de Dios, T. Tavares, M.A. Sanromán, M. Pazos, J. Ind. Eng. Chem. 27 (2015) 276 – 282.

[40] Y. Dong, W. Dong, Y. Cao, Z. Han, Z. Ding, Preparation, Catal. Today. 175 (2011) 346 – 355.

[41] E. Rosales, O. Iglesias, M. Pazos, M.A. Sanromán, J. Hazard. Mater. 213-214 (2012) 369 – 377.

[42] H. Kim, H. J. Hong, J. Jung, S. H. Kim, J. W. Yang, J. Hazard. Mater. 176 (2010) 1038 – 1043.

[43] S. Barrecaa, J. J. V. Colmenares, A. Pace, S. Orecchio, C. Pulgarin, J. Photochem. Photobiol. A: Chem. 282 (2014) 33–40.

[44] O. Iglesias, J. Gómez, M. Pazos, M.Á. Sanromán, Appl. Catal. B: Environ. 144 (2014) 416 – 424.

[45] D. H. Caldwell, R. B. Adams, J. Am. Water. Works. Assoc. 38 (1946) 727–730.

[46] F. Fourcade, T. Tzédakis, A. Bergel, Chem. Eng. Sci. 58 (2003) 3507–3522.

[47] G. Zhang, Y. Zhou, F. Yang, J. Electrochem. Soc. 162 (2015) 357–365.

[48] X. Hua,b, B. Liua, Y. Denga, H. Chena, S. Luoa, C. Suna, P. Yanga, S. Yanga, Appl. Catal. B: Environ. 107 (2011) 274–283

[49] Y. Wang, H. Zhao, S.Chai, Y. Wang, G. Zhao, D. Li, Chem. Eng. J. 223 (2013) 524–535.

[50] M. Sun, X. R. Ru, L. F. Zhai, Appl. Catal. B: Environ. 165 (2015) 103–110.

[51] M. Samah M., S. Merabet, M. Bouguerra, M. Bouhelassa, S. Ouhenia, A. Bouzaza, Kinet. Catal. 52 (2011) 34–39.

[52] E. Brillas, M. A. Ban˜os, M. Skoumal, P. L. Cabot, J. A. Garrido, R. M. Rodríguez, Chemosphere. 68 (2007) 199–209.

[53] A. Dhaouadi, L. Monser, N. Adhoum, Electrochimica. Acta. 54 (2009) 4473–4480

[54] C. C. Su, C. A. Cada, M. P. Dalida, M. C. Lu, Sep. Purif. Technol. 120 (2013) 43–51.

[55] M. Umar, H. A. Aziz, M. S. Yusoff, Waste. Manage. 30 (2010) 2113–2121.

[56] M. S. Lucas, J. A. Peres, Dyes. Pigm. 71 (2006) 236 –244.

[57] Y. J. Shih, Y. J. Huang, Y. H. Huang, Sustain. Environ. Res. 2011 (21) 389–393.

[58] M. D. G. de Luna, M. L. Veciana, C. C. Suc, M. C. Luc, J. Hazard. Mater. 217–218 (2012) 200–207.

[59] A. Dhaouadi, N. Adhoum, J. Electroanal. Chem. 637 (2009) 33–42.

[60] Q. Wang, A.T. Lemley, Environ. Sci. Technol. 35 (2001) 4509 –4514.

[61] A. Wang, Y.Y. Li, A. L. Estrada, Appl. Catal. B: Environ. 102 (2011) 378 –386.

[62] F. Jean-Marie, F. Florence, G. Florence, S. Isabelle, F. Didier, A. Abdeltif, C. R. Chim. 18 (2015) 32–38.

[63] A. Dirany, I. Sires, N. Oturan, M.A. Oturan, Chemosphere. 81 (2010) 594– 602.

[64] M. Panizza, A. Barbucci, M. Delucchi, M. P. Carpanese, A. Giuliano, M. Cataldo-Hernandez, G. Cerisola, Sep. Purif. Technol. 118 (2013) 394–398.

[65] M. Perez, F. Torrades, J. A. Garcia-Hortal, X. Domenech, J. Peral, Appl. Catal. B: Environ. 36 (2002) 63–74.

[66] M. Panizza, G. Cerisola, Water Res. 35 (2001) 3987–3992.

[67] M. Skoumal, R.M. Rodríguez, P.L. Cabot, F. Centellas, J.A. Garrido, C. Arias, E. Brillas, Electrochim. Acta. 54 (2009) 2077–2085.

[68] L. Feng, N. Oturan, E. D. van Hullebusch, G. Esposit, M. A. Oturan, Environ. Sci Pollut. Res. 21 (2014) 8406 –8416.

[69] C. González-Vargas, R. Salazar, I. Sirés, J. Electrochem. Sci. Eng. 4 (2014) 235–245.

[70] D. Mansour, F. Fourcade, S. Huguet, I. Soutrel, N. Bellakhal, M. Dachraoui, D. Hauchard, A. Amrane, Int. Biodeter. Biodegr. 88 (2014) 29–36.

[71] V. S. Antonin, S. Garcia-Segura, M. C. Santos, E. Brillas, J. Electroanal. Chem. 747 (2015) 1–11.

[72] L. E. de-Bashana, M. Morenoa, J. P. Hernandeza, Y. Bashan, Water Res. 36 (2002) 2941–2948.

[73] Y. C. Chung, C. Huang, C. P. Tseng, Biotechnol. Prog. 13 (1997) 794−798.

[74] S. S. Johansen, D. Licht, E. Arvin, H. Mosbæk, Appl. Microbiol. Biotechnol. 47(1997) 292 – 300.

[75] E. L. Madsen, J. M. Bollag, Arch. Microbiol. 151 (1988) 71–76.

Legend

Figure 1. (a) Digital photo of Fe-alginate gel beads, (b) SEM micograph and (c) EDS images of the dry produced Iron entrapped Ca-alginate beads.

Figure 2. EDS spectrum of iron entrapped Ca-alginate bead.

Figure 3. Adsorptive behavior of indole (Experimental conditions: no electrode polarization, Fe-ABs =50 mg, pH=3, $[Indole]_0$ =20 mg L^{-1}, working volume = 250 mL), and its degradation behavior under EF and PEF processes (Experimental conditions: $[Na_2SO_4]$ = 0.1 M, 200 mg L^{-1} Fe-ABs, pH= 3.0, j = 0.53 $mA.cm^{-2}$, working volume of 250 mL, $[Indole]_0$ =20 mg L^{-1}, Air flow rate = 0.25 mL min^{-1}**,** UVA irradiation of 360 nm for the PEF process).

Figure 4. Effect of the Fe-ABs dosage on the indole degradation by the electro-Fenton treatment. Experimental conditions: $[Na_2SO_4]$ = 0.1 M, pH= 3.0, j = 0.53 $mA.cm^{-2}$, working volume of 250 mL, $[Indole]_0$ =20mgL^{-1}, Air flow rate = 0.25 mL min^{-1}

Figure 5. Effect of the applied density on indole removal during electro-Fenton treatment in the presence of 200 mg L^{-1} Fe-ABs. Experimental conditions: [Na_2SO_4] = 0.1M, pH= 3.0, working volume of 250 mL, $[Indole]_0$ =20 mg L^{-1}, Air flow rate = 0.25 mL min^{-1}

Figure 6. Mineralization of indole solutions (20 mg L^{-1}) by (EF-Fe-ABs) Electro-Fenton and (PEF-Fe-ABs) photoelectro-Fenton with UVA light of λ_{max} = 360 nm. Experimental conditions: [Na_2SO_4] = 0.1 M, pH= 3.0, j = 0.53 mA.cm^{-2}, working volume of 250 mL, $[Indole]_0$ =20 mg L^{-1}, Air flow rate = 0.25 mL $min^{-1}$and 200 mg L^{-1} Fe-ABs .

Figure 7. Effect of current intensity on NPOC removal (A) and time evolution of electrical energy consumption (B) and current efficiency during electro-Fenton treatment (Experimental conditions: [Na_2SO_4] = 0.1 M, pH= 3.0, working volume of 250 mL, $[indole]_0$ =20 mg L^{-1}, Air flow rate = 0.25 mL $min^{-1}$and Fe-ABs = 200 mg L^{-1}).

Figure 8. (a) LC–MS profile of indole and its derivatives at different times (initial, 60 min, 120, 180 and 240 min) and (b) time–course of indole derivatives during the EF-Fe-ABs degradation of 200 mg L^{-1} indole aqueous solution. Experimental conditions: [Na_2SO_4] = 0.1 M, pH= 3.0, j = 0.27 mA cm^{-2}, working volume of 250 mL, $[Indole]_0$ =20 mg L^{-1}, Air flow rate = 0.25 mL min^{-1},[Fe-ABs] = 200 mg L^{-1}.

Figure 9. Plausible degradation pathway of indole by the EF-Fe-ABs process.

Figure 10. Degradation profile of indole using the heterogeneous electro-Fenton process with recycling of the iron alginate beads, Fe-ABs. Experimental conditions: [Na_2SO_4] = 0.1 M, pH= 3.0, j = 0.53 mA cm^{-2}, working volume of 250 mL, $[Indole]_0$ = 20 mg L^{-1}, Air flow rate = 0.25 mL min^{-1}, Fe-ABs = 200 mg L^{-1}.

Table 1. Mass diameter and Fe content of wet and dry Fe alginate bead.

C_{SA}(%w/w)[a]	m_{wet}(mg)	m_{dry}(mg)	D_{wet} (mm)	D_{dry} (mm)	$C_{Fe\text{-}bead}$ (mg) (±SD)
3.0	35.23	1.25	4.00	1.25	0.40±0.03

[a]C_{SA} : The concentration of sodium alginate

Table 2.LC–MS/MS identification of the chemical structure, retention time and main mass fragmentation values of identified indole intermediates formed during the EF-Fe-ABs process.

Identification number	Compound	Formula	Structure	tr (min)	M (g/mol)	Main mass fragmentation value (m/z)
1	Indole	C_8H_7N	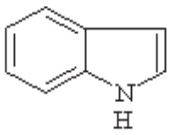	4.48	117	ES+ :118/91 ES- : 116/89
2	Oxindole	C_8H_7NO	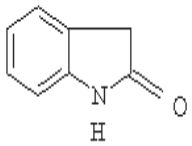	2.87	133	ES+ :134/105,9 ES- : 132
3	Isatin	$C_8H_5NO_2$	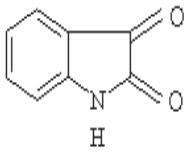	2.56	147	ES+ : 148/120/92 ES- :146 /118/90.9
4	Dioxindole	$C_8H_7NO_2$	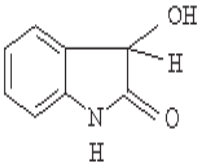	1.79	149	ES- : 148/119.9/91.9
5	AnthranilicAcid	$C_7H_7NO_2$	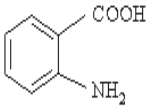	2.8	137	ES+:/138/119,9/91,9 ES- :136/91,9

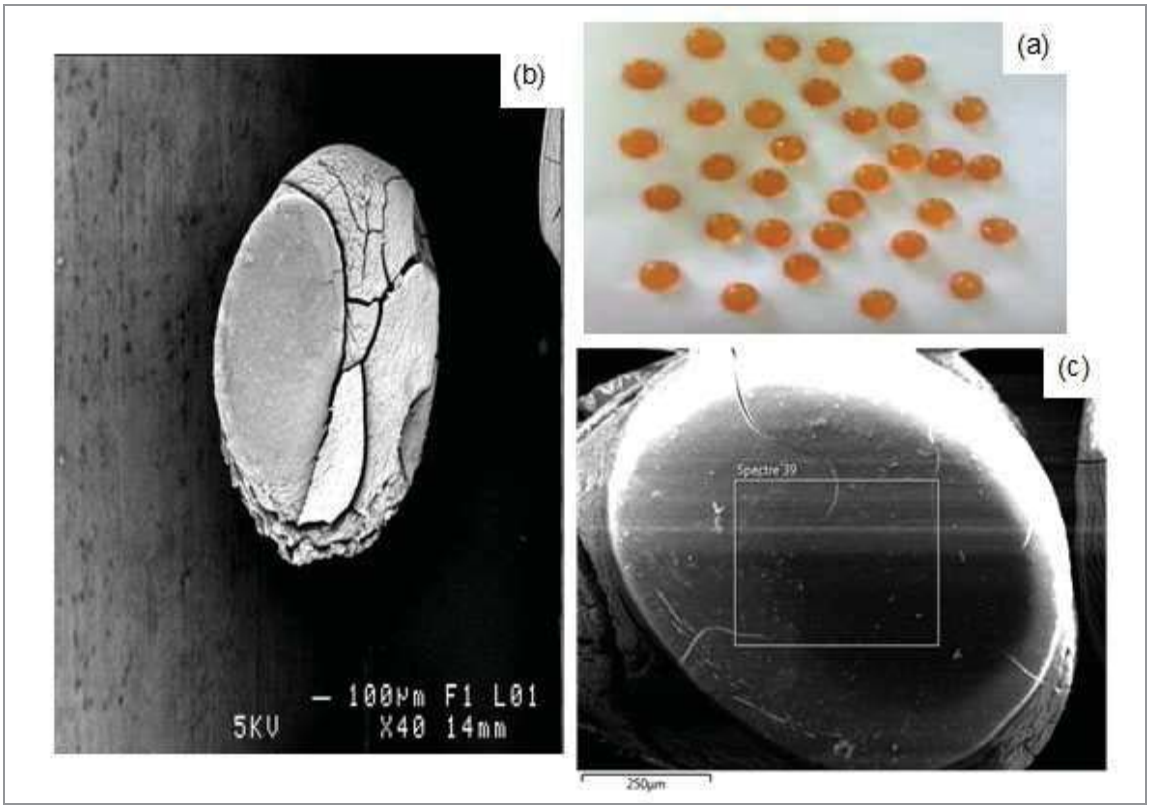

Figure 1

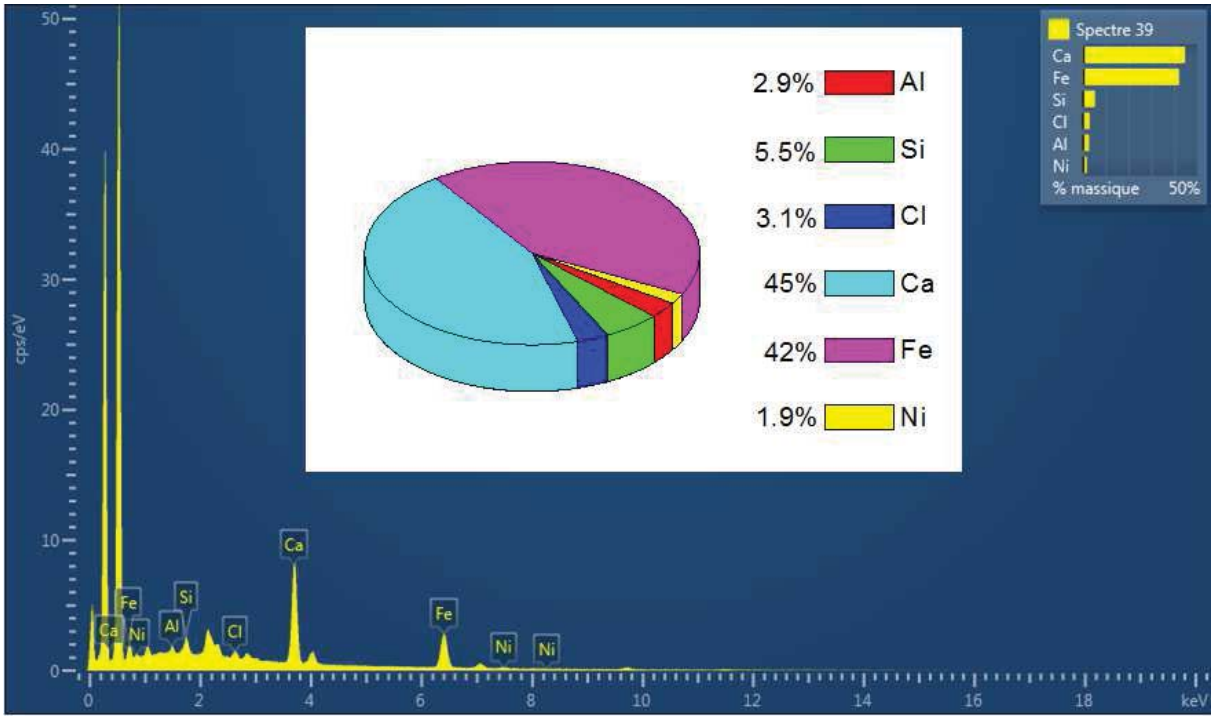

Figure 2

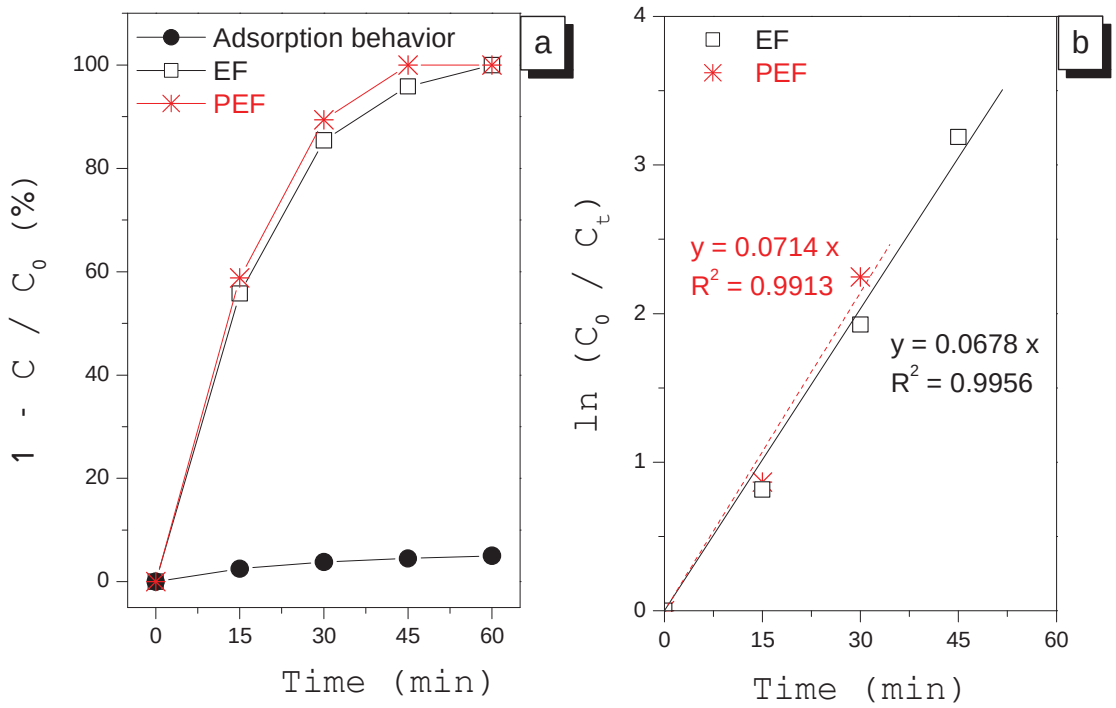

Figure 3

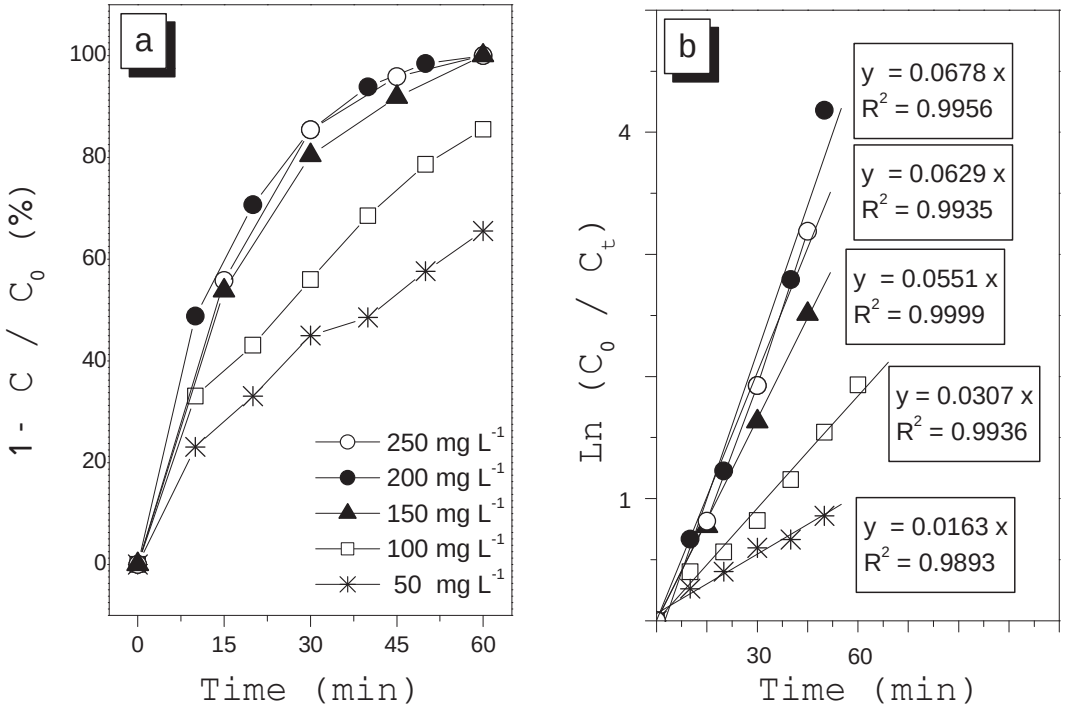

Figure 4

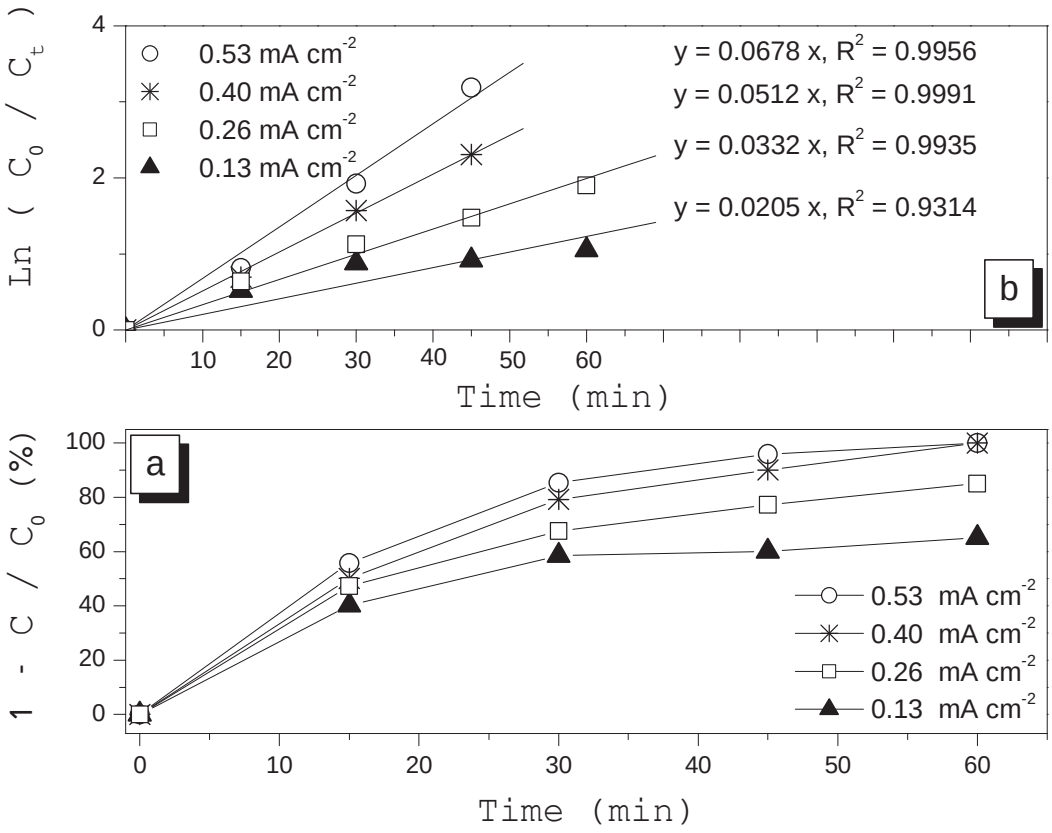

Figure 5

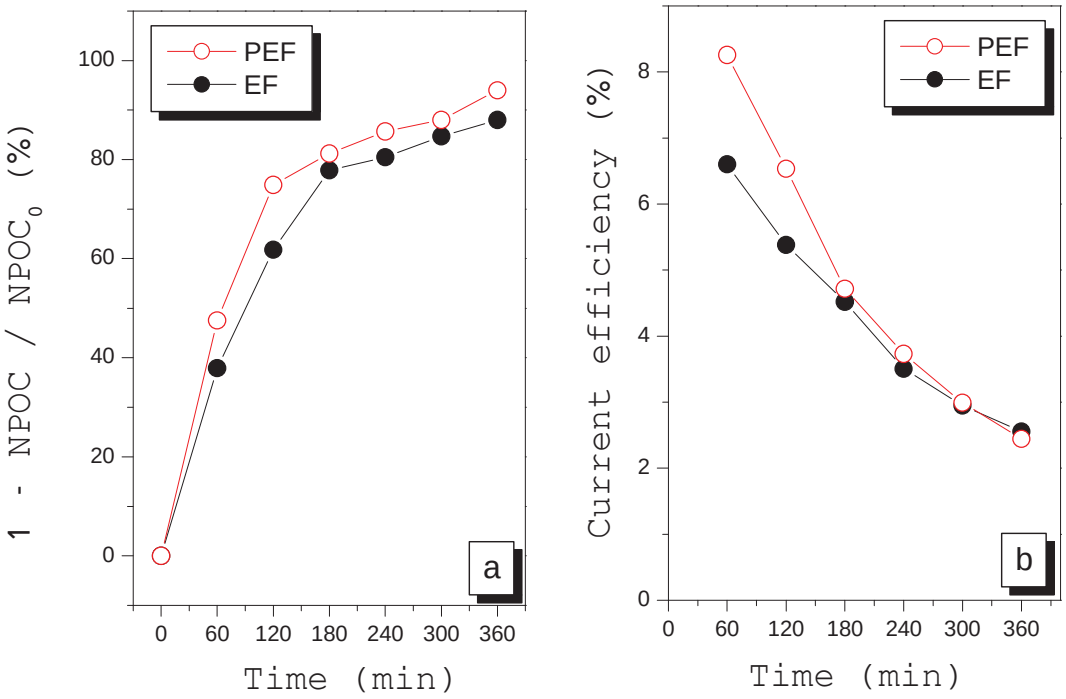

Figure 6

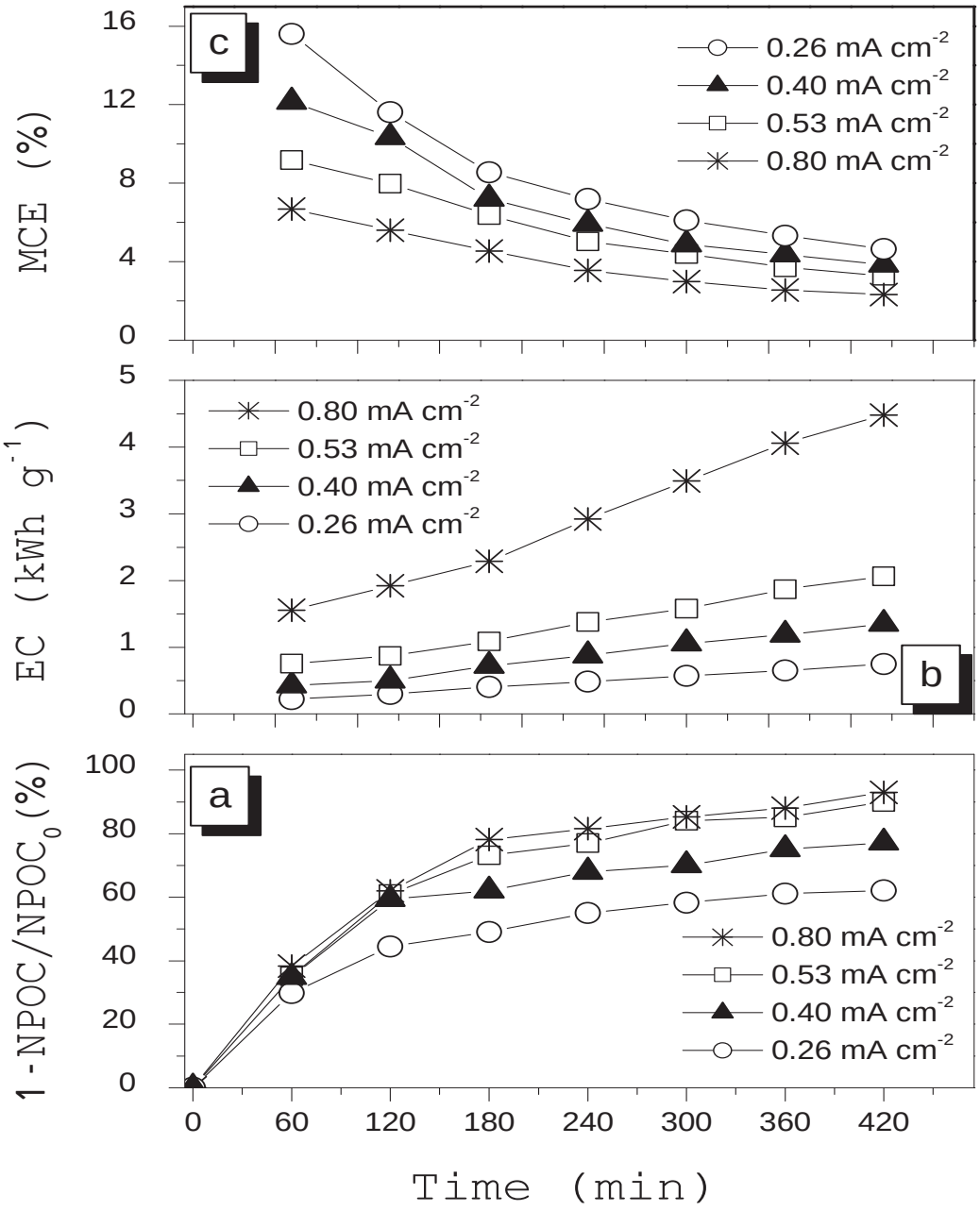

Figure 7

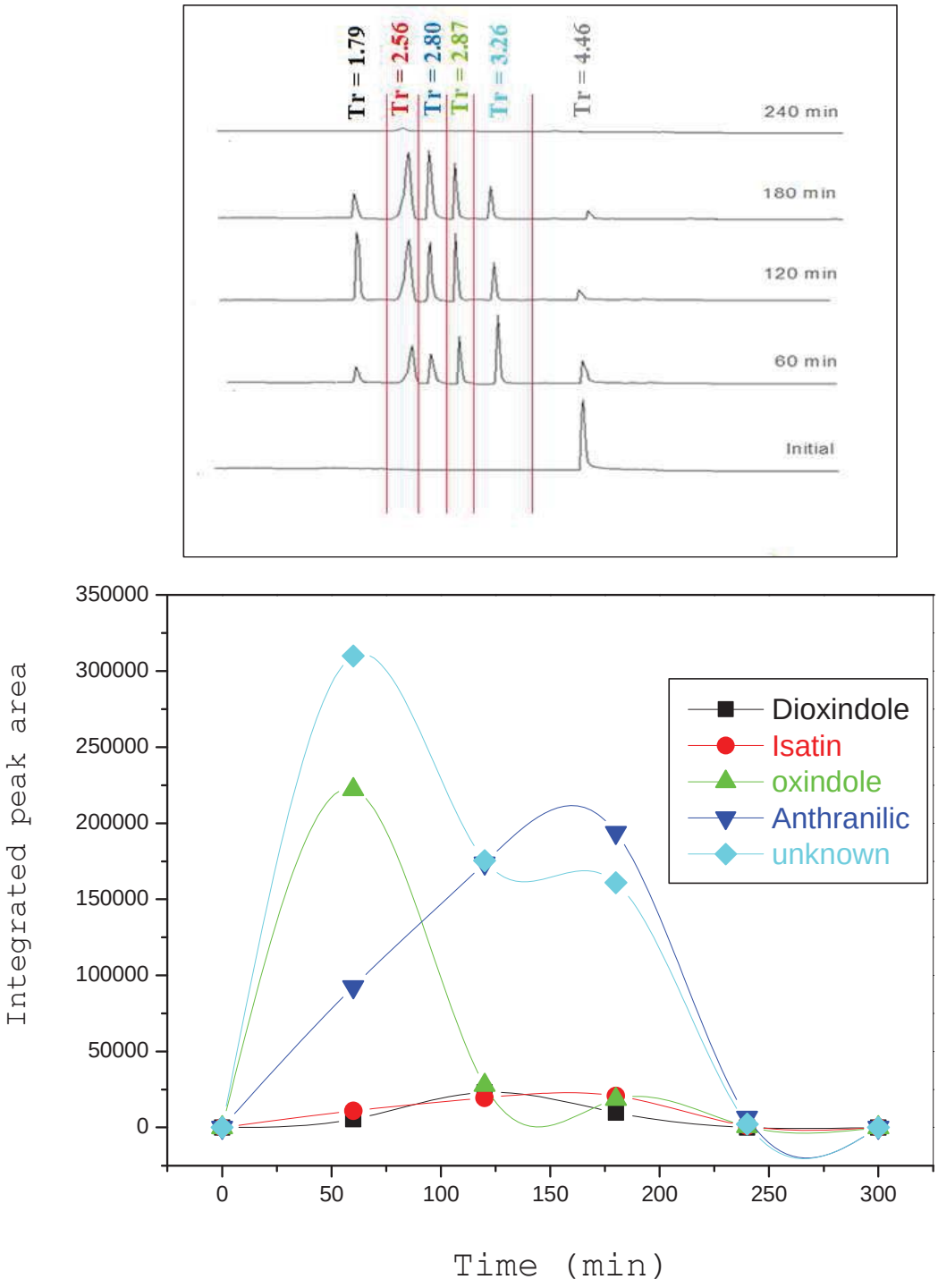

Figure 8

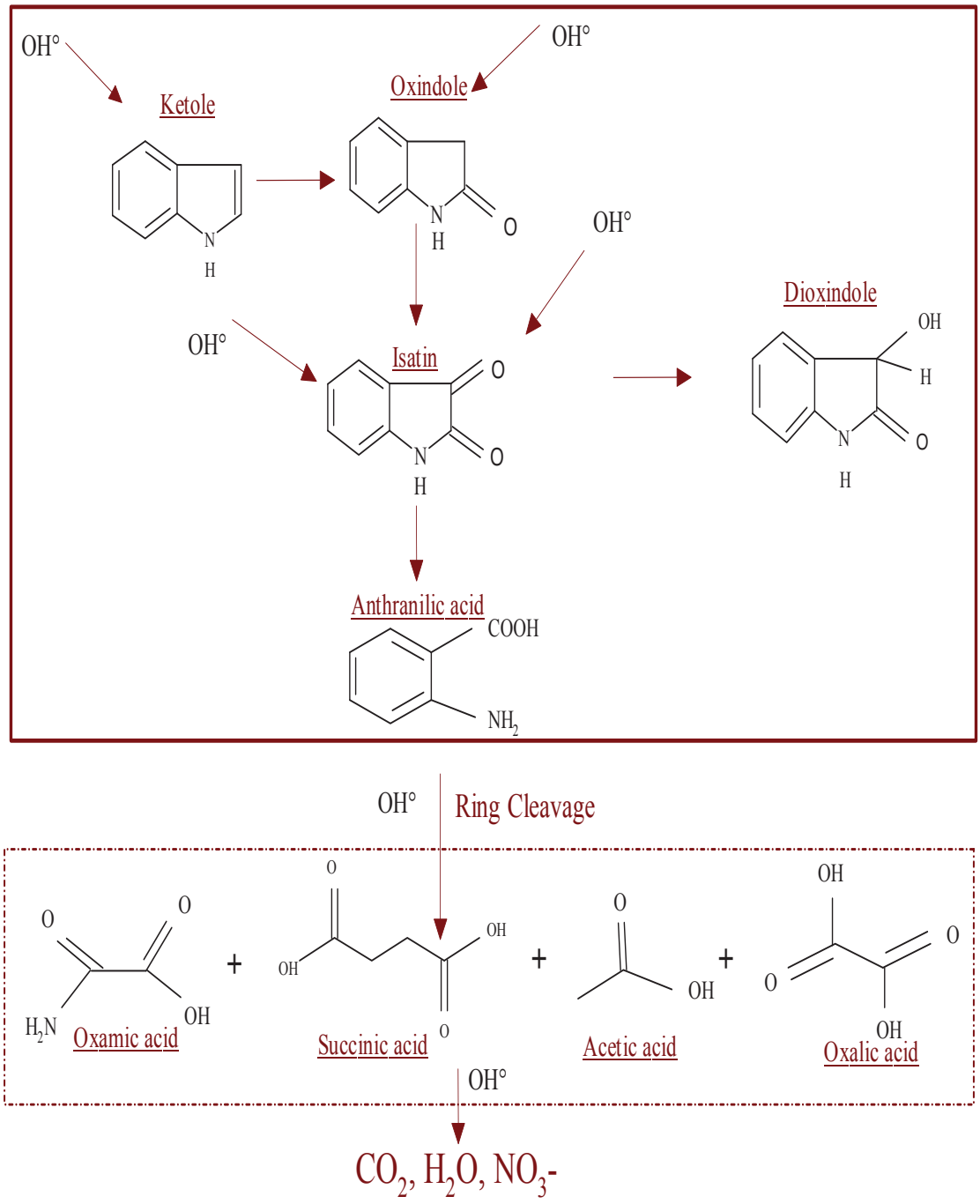

Figure 9

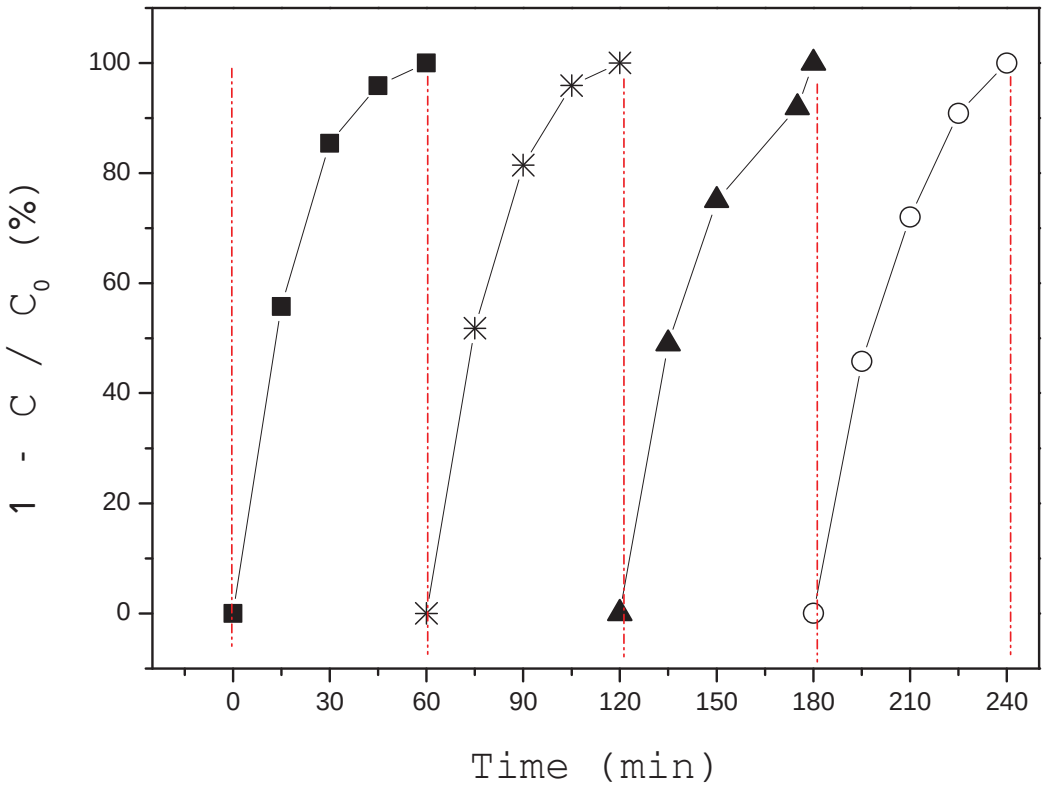

Figure 10